OPERATION OF AIR-BREATHING HYDROGEN-FUELED ROTATING DETONATION ENGINE IN SUPERSONIC FLIGHT CONDITIONS: NUMERICAL SIMULATION

A. V. Dubrovskii, S. M. Frolov, V. S. Ivanov, and A. E. Zangiev

N. N. Semenov Institute of Chemical Physics
Russian Academy of Sciences
Moscow, Russia
e-mail: smfrol@chph.ras.ru

Three-dimensional (3D) numerical simulations demonstrate the feasibility of the continuous-detonation process in an annular combustor of a ramjet power plant operating on hydrogen as fuel and air as oxidant in conditions of flight at a Mach number of $M_0 = 5.0$ and an altitude of 20 km. Conceptual schemes of an axisymmetric power plant with a supersonic intake, divergent annular combustor, and outlet nozzle with a frustoconical central body are proposed. Calculations of the characteristics of the internal and external flows, with consideration given to the finite rate of turbulent-molecular mixing of the fuel mixture components with each other and with the combustion products as well as the finite rate of chemical reactions and the viscous interaction of the flow with the bounding surfaces have shown that in these flight conditions, the engine of such a power plant can operate with one detonation wave traveling in the annular channel at an average velocity of 1695 m/s, which corresponds to a detonation wave rotation frequency of 1350 Hz, and has the following performance characteristics: the thrust 10.7 kN; specific thrust 0.89 kN·s/kg; specific impulse 1210 s; and specific fuel-consumption 0.303 kg/(N·h).

Introduction

Controlled detonation combustion is a way to implement the most efficient thermodynamic cycle of conversion of the chemical energy of

fuel into useful work [1]. The theoretical coefficient of performance (COP) of detonation power plants may exceed the COP of existing plants by 15%–20% [2–4]. The possibility of organizing a continuous spin detonation (CSD) in a ramjet engine with supersonic incident flow was considered in [5]. A numerical solution for a hydrogen–oxygen (not hydrogen–air!) mixture in an annular cylindrical combustor operating at incoming flow Mach numbers of up to $M_0 = 3.0$ was obtained. Later [6], the two-dimensional unsteady problem of CSD in an annular combustor considered in [5] was generalized to take into account the preliminary isentropic or shock-wave compression of the supersonic flow of a hydrogen–oxygen (not air!) mixture in the inlet diffuser. Based on the calculation results, the authors of [6] have drawn the conclusion that the realization of CSD in an annular hydrogen–oxygen combustor is limited from above by an incoming supersonic flow Mach number of $M_0 = 4.0$. This conclusion contradicts the results of [7], where the feasibility of CSD at Mach numbers M_0 up to M_{CJ} is considered. In addition, the findings of [6] contradict those of [8], in which 3D calculations demonstrated the feasibility of realization of CSD at a supersonic velocity of premixed hydrogen–air (not oxygen!) mixture in an annular combustor with a channel width of 20 mm corresponding to a flight at $M_0 = 4.0$. Lastly, the conclusion drawn in [6] contradicts to [9], where the results of successful experimental studies of CSD in a hydrogen–air (not oxygen!) mixture in conditions simulating a supersonic flight at $M_0 = 4.0$ are reported.

The aim of the present work was to explore the possibility of organizing the process of continuous detonation in an axisymmetric annular combustor of a ramjet engine in flight with $M_0 = 5.0$ at an altitude of 20 km operating on hydrogen and air, which can be supplied to the combustor premixed [8] or separately [10–12].

Power Plant

Figure 1 shows a schematic of a hydrogen-fueled power plant in flight conditions. The power plant consists of supersonic air intake *1*, divergent combustor *2*, and outlet nozzle *3* with frustoconical central body *4* with an apex angle of 15°. The outer diameter of the combustor is 400 mm. Two configurations of the power plant with a total

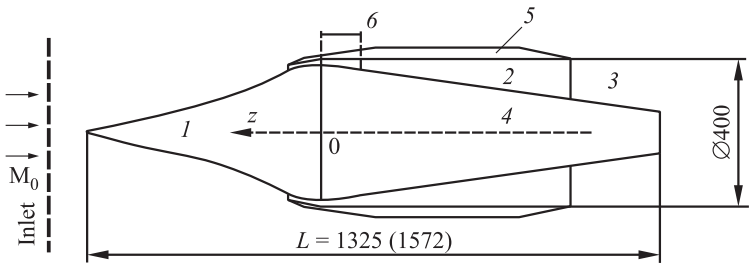

Figure 1 Schematic diagram of a ramjet power plant with a continuous-detonation combustor (for details, see the text). Dimensions are in millimeters

length of 1325 and 1572 mm but with different lengths of central body *4* and cowling *5* have been considered.

On the left (inlet) boundary of the computational domain, the velocity of the fluid and its temperature corresponding to the standard atmospheric conditions, as well as nonzero parameters of (weak) turbulence, are specified.

Mathematical Model and Calculation Procedure

The physicochemical processes involved are simulated using the mathematical model and calculation procedure described in detail in [13]. Here, a recapitulation of their main features is given. The flow of a viscous compressible gas is described by the 3D unsteady Reynolds-averaged Navier–Stokes, energy, and species continuity equations for a multicomponent mixture. The turbulent fluxes of mass, momentum, and energy were described within the framework of the standard k–ε turbulence model for compressible flows. Since all the physicochemical processes in the simulated combustor occur within a very short time, the contributions from frontal combustion (laminar and/or turbulent) to the chemical sources in the energy and species continuity equations were disregarded. The contributions from the bulk reactions to these chemical sources were determined using the particle method (PM).

The PM allows determining the rates of chemical reactions in a turbulent flow without using any hypotheses concerning the impact of tur-

bulent fluctuations of temperature and reactant concentrations on the mean reaction rate. In the PM algorithm, the instantaneous local states of a turbulent reacting flow are represented as a set of interacting (Lagrangian) particles. For each particle, a system of equations of conservation of chemical components, momentum, and energy is solved, with the classical models of relaxation to the mean [14] being used to determine the flux (exchange) terms. The equations of the model are closed by the caloric and thermal equations of state of an ideal gas mixture with variable heat capacity, as well as by initial and boundary conditions. All the thermophysical parameters of the gas were considered variable.

The governing equations are solved by using the SIMPLE (semi-implicit method for pressure linked equations) method — Monte-Carlo method coupled algorithm. The chemical source terms are calculated using an implicit scheme with internal integration time step. In simulations, the oxidation of hydrogen is described by a validated one-step reaction scheme with tabulated Arrhenius parameters.

In the calculations with the premixed flow of hydrogen–air mixture, chemical transformations in the gas are artificially suppressed in the external flow everywhere while in the internal flow up to section *6* (located at $z \leq 0$) by setting zero reaction rates. Moreover, one of the objectives of these calculations is to determine such a location of section *6* that would prevent the formation of a detached shock wave. When searching for the position of section *6*, it is assumed that for the separate supply of air and hydrogen, the belt of hydrogen injection must be located upstream of section *6* because it takes a finite time to mix hydrogen and air.

In the calculations with separate supply of hydrogen and air, the power plant of the same size is then used to obtain the characteristics of the flow-past (internal and external) of the power plant by an infinite incoming air stream. On the left (inlet) boundary of the computational domain, the velocity of the air and its temperature characteristic of the standard atmospheric conditions are specified, as well as nonzero parameters of (weak) turbulence. Hydrogen is fed into the combustor radially from the central body through a 2.6-millimeter slot in section *6* at $z \leq 0$ (see Fig. 1). In this case, chemical conversion is nowhere artificially suppressed. The standard atmosphere parameters at the altitude of 20 km are as follows: static pressure 5529 Pa and static temperature 216.7 K.

The calculation begins with purging the power plant by the incoming flow of a hydrogen–air mixture (or air, with hydrogen being fed through a slot in section *4*) for 0.1 ms, a time required to form in the combustor a reaction mixture layer of sufficient thickness. Next, the procedure of detonation initiation starts, which consists in rapidly burning all the particles in the initiator area ($50 \times 50 \times 30$ mm), which is located in the active layer. The burning of particles increases the pressure in the initiator area, thereby producing an initiating shock wave propagating in the annular channel of the combustor in all directions.

It should be noted that the predictive ability of the above model was previously tested using the experimental data on continuous detonation of a hydrogen–air mixture reported by a research team from the Lavrent'ev Institute of Hydrodynamics SB RAS [15] and by our group [11, 16] obtained in annular combustors with outer diameters of 306 [15, 17] and 406 mm [10, 11, 16]. The tests showed good agreement with the experimental and theoretical results in the number of simultaneously rotating detonation waves, detonation wave velocity, detonating layer height, pressure in the combustor, and the thrust developed.

Calculation Results

Table 1 lists the variants of calculations to be discussed below. In variants 1–4, a stoichiometric hydrogen–air mixture is supplied to the intake of the power plant. Variant 1 corresponds to a power plant of the first configuration, with a total length of 1325 mm, whereas variants 2–4 to a power plant of second configuration, with a total length of 1572 mm, differing in wall temperature T_w (273, 1000, and 1000 K for variants 2, 3, and 4, respectively) and computational grid cell size (0.7, 0.7, and

Table 1 Variants of calculations

Variant	Scheme	Grid (10^{-6} cells)	Premixed composition	Separate supply	T_w, K
1	1	0.6	+	−	273
2	2	0.7	+	−	273
3	2	0.7	+	−	1000
4	2	2.2	+	−	1000
5	2	0.7	−	+	1000

2.2 million cells for variants 2, 3, and 4, respectively). Thus, a comparison of the calculation results for variants 1–4 makes it possible to identify the advantages and disadvantages of a particular configuration of the power plant, evaluate the effect of the wall temperature on the performance characteristics of the process, and assess the influence of the computational grid on the results. Variant 5 is identical to variant 3 but differs from the latter in that the air is fed through the intake of the power plant, while hydrogen is fed into the combustor from the external wall in section *4* (see Fig. 1) at a rate of 0.9 kg/s as an annular jet directed perpendicular to the axis of the power plant.

Thrust characteristics: Definitions

Distinguish here between the notions "power plant" and "engine" as is customary in the literature on the subject. The term "power plant" means a device consisting of an engine, air intake, nozzle, and other elements. The term "engine" means the part of the power plant that produces jet thrust. First, let us consider the characteristics of the engine. Table 2 lists the calculated values of the detonation wave rotation frequency, thrust, specific thrust, specific impulse, and specific fuel consumption for variants 1–5. These parameters are calculated as follows:

– the detonation wave rotation frequency is calculated by the formula

$$f = \frac{nD}{\pi d}$$

Table 2 Thrust characteristics of the engine calculated in variants 1–5

Variant	Detonation rotation frequency, Hz	Thrust, kN	Specific thrust, kN·s/kg	Specific impulse, s	Specific fuel consumption, kg/N/h
1	1110	3.9	0.57	1990	0.185
2	1130	4.6	0.67	2350	0.157
3	1150	4.5	0.65	2300	0.160
4	1210	4.4	0.64	2250	0.164
5	1350	10.7	0.89	1210	0.303

where n is the number of detonation waves simultaneously rotating in the annular channel; D is the detonation wave velocity, and d is the diameter of the combustor outer wall;

– the thrust F of the engine is defined as the resultant of the forces of relative pressure P_{rel} and friction T_f created on all solid surfaces of the engine by the gas flowing inside the engine:

$$F = \int_S (P_{\text{rel}} + T_f)\, dS\,, \quad P_{\text{rel}} = P_{\text{abs}} - P_{\text{in}}\,;$$

– the specific thrust of the engine is defined as the ratio of its thrust to the mass flow rate of air:

$$F_{\text{sp}} = \frac{F}{\dot{m}_{\text{air}}}\,;$$

– the specific impulse of the engine is defined as the ratio of its thrust to the weight flow rate of fuel:

$$I_{\text{sp}} = \frac{F}{g\dot{m}_{\text{fuel}}}\,;$$

– the specific fuel consumption is defined as the ratio of the hourly mass fuel consumption to the engine thrust:

$$C_{\text{sp}} = \frac{3600\dot{m}_{\text{fuel}}}{F}\,.$$

Let us now consider the characteristics of the power plant. Table 3 lists the calculated values of the effective thrust force and the drag force of the power plant for variants 1–5. These parameters are calculated as follows:

– the effective thrust F_{ef} is defined as the resultant of the forces of absolute pressure P_{abs} and friction T_f created on all solid surfaces of power plant by the gas flowing both inside the engine and over the external surface of the power plant:

$$F_{\text{ef}} = \int_S (P_{\text{abs}} + T_f)\, dS$$

where S is the surface vector. The positive value of the effective thrust of the power plant means that the resulting force is directed

Table 3 Thrust characteristics of the power plant engine calculated for variants 1–5

Variant	Effective thrust, kN	External drag force, kN
1	1.09	−2.81
2	1.89	−2.71
3	1.79	−2.71
4	1.66	−2.74
5	6.41	−4.29

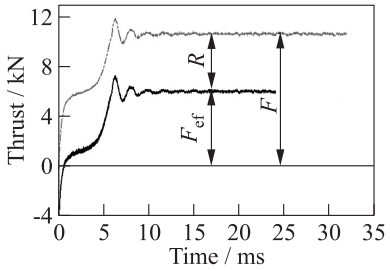

Figure 2 Approach of the engine thrust F and the efficient thrust of the power plant to their steady-state values for variant 5

along the z axis from right to left (in the direction of flight, see Fig. 1).

– the drag force R of the power plant is defined as the resultant of the forces of relative pressure P_{rel} and friction T_f produced on all the solid surfaces of the power plant by the gas flow around the power plant:

$$R = \int_S (P_{\text{rel}} + T_f)\, dS\,.$$

A negative value of the drag force of the power plant means that the resulting force is directed along the z axis from left to right (against the direction of flight, see Fig. 1). For variant 5, as an example, Fig. 2 shows how the thrust of the engine F and effective thrust of the power plant F_{ef} tend to steady-state values in the course of calculations. As can be seen, the difference between the thrust of the engine and the effective thrust of the power plant exactly equals the drag force R of the power plant.

Effect of the configuration of the power plant

In variants 1 and 2 (see Table 1), a combustion mode with one rotating detonation wave inclined at $\sim 60°$ to the engine axis has been established. In both variants, the "base" of the detonation wave is located in

section *6* (see Fig. 1), upstream of which the chemical transformations are artificially suppressed. Examination of the flow structure shows that upstream of section *6*, the flow is supersonic, whereas in the combustor channel, there are large areas of subsonic detonation products. Throughout the outlet section of the combustor ($z = -678.4$ mm), the flow is supersonic. The expansion of detonation products in outlet nozzle *3* (see Fig. 1) leads to a further acceleration of the supersonic flow.

Table 2 shows that the thrust, specific thrust, and specific impulse of the engine in variant 2 are higher (by 18%, 17.5%, and 18%, respectively), while specific fuel consumption is lower (by 15%) than those in variant 1. Table 3 demonstrates that the effective thrust of the power plant in variant 2 is 73% higher and the drag force is 4% lower than those in variant 2. These differences are primarily associated with a fuller expansion of the detonation products inside the engine in variant 2.

Influence of the wall temperature

Similar to variants 1 and 2, in variant 3 (see Table 1), a combustion mode with one rotating detonation wave inclined at $\sim 60^\circ$ to the engine axis has been also established. The higher wall temperature in variant 3 leads to a slight drop in the peak pressures in the detonation wave, which is associated with a decrease in the density of the gas in the near-wall layer. However, the time-average velocity of the detonation wave in the combustor is identical with variant 2: $\sim$ 1420 m/s, a value 28% lower than the thermodynamic detonation velocity ($\sim$ 1970 m/s) for the test mixture. The lower detonation velocity is mainly associated with the lateral expansion of the products and, to a much lesser extent, with the loss of momentum and energy to the chamber walls. Another reason for this is a partial burnout of the mixture in the mixing layers at the interface between the fresh mixture and combustion products, which is also demonstrated by the calculations. Table 2 shows that the combustor wall temperature virtually does not affect the thrust characteristics of the engine, although small reductions in the thrust, specific thrust, and the specific impulse (2%, 3%, and 2%, respectively) and a slight increase in the specific fuel consumption (2%) are observed for variant 3 as compared to variant 2. The data of Table 3 suggest that the higher wall temperature in variant 3 reduces the effective thrust of the power plant by 5%, while the drag force remains unchanged.

Influence of the computational grid

The refinement of the computational grid in variant 4 virtually does not affect the combustion mode and performance characteristics. For example, the time-average total heat fluxes into the outer/inner combustor wall in variants 3 and 4 are $\sim 0.34/0.29$ and $\sim 0.33/0.28$ MW/m^2, respectively, while the time-average values of the detonation velocity in the combustor are slightly different: 1440 m/s for variant 3 and 1520 m/s for variant 4. Nevertheless, grid refinement affects the structure of the mixing layer at the interface between the fresh mixture and combustion products, in which the fuel mixture partially burns out. In variant 4, the energy release zone in the mixing layer is narrower than that in variant 3. This may be the reason for a slightly higher average detonation velocity in variant 4 compared to variant 3.

As can be seen from Tables 2 and 3, the refinement of the computational grid produces almost no effect on the thrust characteristics of the engine. For example, Table 2 shows that thrust, specific thrust, and the specific impulse of the engine in variant 4 are lower by 2%, 1.5%, and 2%, respectively, while the specific fuel consumption is 2.5% higher than that in variant 3. At the same time, Table 3 demonstrates that in variant 4, the effective thrust of the power plant is 7% lower whereas the drag force is 1% higher than those in variant 3.

Effect of the finite mixing time of the fuel components

Figure 3 compares the fields of static pressure calculated in variants 3 and 5 under steady-state flow conditions with one rotating detonation wave in the combustor. In contrast to variant 3 in which a premixed hydrogen–air mixture is fed into the combustor and the chemical transformations are artificially suppressed upstream of section *6* ($z \geq -69.2$ mm), in variant 5, an annular slot was situated at the central body in section *6* ($z = 0$) for supplying hydrogen, which is then mixed with air entering the combustor through the air intake. Hydrogen flows through the annular gap into the combustor at a preset constant flow rate of 0.9 kg/s and temperature of 250 K.

To provide an operation mode with one detonation wave in variant 5, it was necessary to substantially increase the hydrogen-to-air flow rate ratio (7.5%) as compared to that for variant 3 (2.8%). Since

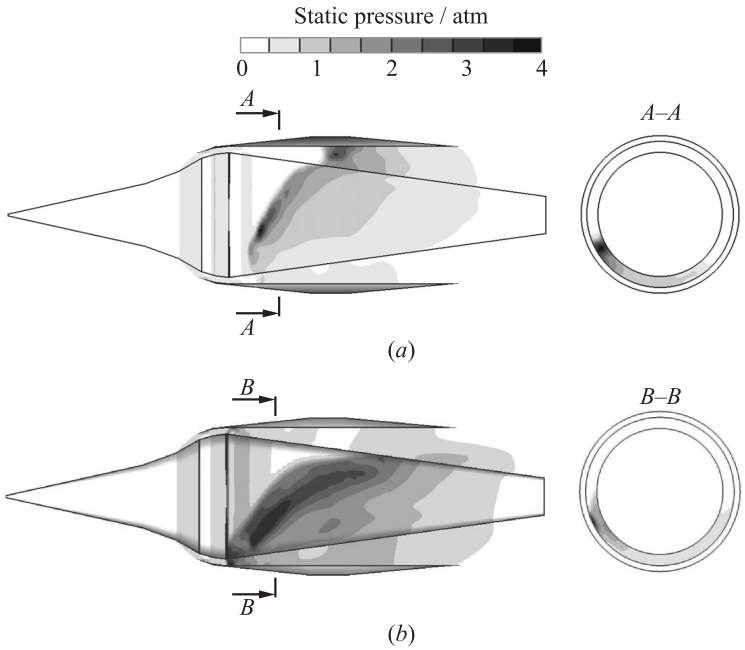

Figure 3 Calculated fields of static pressure on the surface of the central body and in the annular channel of the combustor for variants 3 (*a*) and 5 (*b*). In sections *A*–*A* and *B*–*B*, the detonation wave rotates clockwise

the molecular mixing of hydrogen with air (obligatory condition for the occurrence of chemical transformations!) occurs at a finite rate, the "base" of the detonation wave in variant 5 is shifted downstream of the annular gap for hydrogen supply, whereas the "length" of the detonation wave (its size in the axial direction) is greater than in variant 3.

The first factor creates a situation where the oblique shock wave attached to the detonation wave, traveling upstream, fails to reach the annular gap for hydrogen supply and, therefore, produces no effect on the inlet boundary condition of constancy of hydrogen flow rate through the gap. The fact that the "length" of the detonation wave in variant 5 is greater is associated with the spatial inhomogeneity of the composition of the combustible mixture in the combustor. To illustrate this

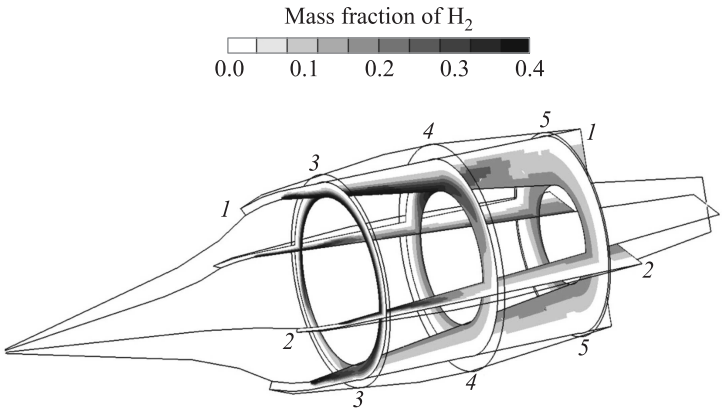

Figure 4 Calculated fields of hydrogen mass fraction in various longitudinal (*1–1* and *2–2*) and transverse (*3–3*, *4–4*, and *5–5*) sections for variant 5

point, Fig. 4 shows the fields of hydrogen mass fraction for five sections of the engine: two longitudinal sections (*1–1* and *2–2*) and three transverse sections (*3–3*, *4–4*, and *5–5*). In transverse sections *3–3*, *4–4*, and *5–5*, local hydrogen equivalence ratio φ ranges from 0 to 12, 10, and 5 (very rich mixtures), respectively, with hydrogen being mainly concentrated near the inner wall of the combustor. Despite a large fraction of unburnt hydrogen in the outlet section of the combustor ($\sim 66\%$ of the total hydrogen consumption), the detonation velocity in variant 5 turned out to be higher than in variant 3 (~ 1695 vs. 1440 m/s) which led to a higher static pressure and static temperature in both the detonation wave and the combustor. Furthermore, in variant 5, the time-average total specific heat fluxes into the outer/inner combustor walls turned out to be higher (1.01/0.60 MW/m^2) than those in variant 3 (0.34/0.29 MW/m^2).

The calculations show that upstream of section *6* (see Fig. 1), the flow is supersonic, whereas in the combustor ($z < 0$), there are zones of subsonic flow of detonation products, with the length and shape of these zones varying radially. In the outlet section of the combustor ($z = -678.4$ mm), the flow is supersonic throughout the annular channel. The expansion of detonation products in outlet nozzle *3* (see Fig. 1) leads to a further acceleration of the supersonic flow.

The data given in Tables 2 and 3 make it possible to compare the calculated values of the thrust and specific characteristics of the engine for variants 3 and 5. Accounting for the finite time of mixing of the fuel components in variant 5 leads to a significant increase in the specific fuel consumption (1.9-fold) and to a decrease in the specific impulse (1.9-fold); the specific thrust, however, increases by a factor of 1.37. The main reason for the reduction of the specific impulse of the engine (from 2300 s for variant 3 to 1210 s for variant 5) is an incomplete hydrogen burnout. The specific impulse can be increased by changing the mode of hydrogen supply into the combustor. As regards the effective thrust and drag force of the power plant, these characteristics for variant 5 turned out to be significantly higher than for variant 3 because of a higher density of the incoming air compared with the density of the incoming stoichiometric hydrogen–air mixture.

Concluding Remarks

Thus, multivariant 3D numerical simulations demonstrated the feasibility of the continuous-detonation process in an annular combustor of a ramjet power plant operating on hydrogen as fuel and air as oxidant in conditions of flight at a Mach number 5.0 and an altitude of 20 km. Conceptual scheme of an axisymmetric power plant, 400 mm in external diameter and 1.3 to 1.5 m in length, with a supersonic intake, divergent annular combustor, and outlet nozzle with a frustoconical central body were proposed.

Calculations of the characteristics of the internal and external flows, with consideration given to the finite rate of turbulent-molecular mixing of the fuel mixture components with each other and with the combustion products as well as the finite rate of chemical reactions and the viscous interaction of the flow with the bounding surfaces have shown that in these flight conditions, the engine of such a power plant can have the following performance characteristics: the thrust 10.7 kN, specific thrust 0.89 (kN·s)/kg; specific impulse 1210 s; and specific fuel-consumption 0.303 kg/(N·h). In this case, the combustor can operate with one detonation wave traveling in the annular channel at an average velocity of 1695 m/s which corresponds to a detonation wave rotation frequency of 1350 Hz.

It was shown that an operating combustor has regions of subsonic flow of detonation products, but the flow is supersonic throughout its outlet section. These results contradict the conclusion drawn in [6] based on two-dimensional simulations, which claims that the maximum velocity of an aircraft with a continuous-detonation engine operating on a premixed $2H_2 + O_2$ mixture cannot exceed $M_0 = 4.0$. First, our 3D calculations were performed not for a hydrogen–oxygen mixture, but for a hydrogen–air mixture, which has a much lower detonability. Second, in our calculations, the fuel (hydrogen) and oxidant (air) were fed separately. Third, there was found an operation mode with a positive effective thrust in flight with a Mach number of $M_0 = 5.0$. In the authors' opinion, the reasons for the differences between their calculation results and those reported in [6] may be associated with the two-dimensional approximation of the flow and with the boundary conditions at the outlet section of the annular combustor. Approximating the flow in an annular combustor by its "unrolling" onto a plane without regard for radial inhomogeneities must distort the real 3D pattern of the flow.

Acknowledgments

This work was supported by the Ministry of Education and Science of the Russian Federation under State Contract No. 14.609.21.0002 (contract ID RFMEFI60914X0002).

References

1. Zel'dovich, Ya. B. 1940. K voprosu ob energeticheskom ispol'zovanii detonatsionnogo goreniya [To the question of energy use of detonation combustion]. *Zh. Tekhn. Fiz.* [J. Tech. Phys.] 10(17):1455–1461.
2. Heiser, W. H., and D. T. Pratt. 2002. Thermodynamic cycle analysis of pulse detonation engines. *J. Propul. Power* 18(1):68.
3. Frolov, S. M., A. E. Barykin, and A. A. Borisov. 2004. Termodinamicheskiy tsykl s detonatsionnym szhiganiem topliva [Thermodynamic cycle with detonation combustion of fuel]. *Russ. J. Chem. Phys.* 23(3):17–25.
4. Chvanov, V. K., S. M. Frolov, and L. E. Sternin. 2012. Zhidkostnyy detonatsionnyy raketnyy dvigatel' [Liquid-propellant detonation rocket engine]. *Trudy NPO Energomash imeni Akademika V. P. Glushko* [Herald of NPO Energomash named after Academician V. P. Glushko]. Moscow: NPO Energomash named after Academician V. P. Glushko. 29:4–14.

5. Zhdan, S. A. 2008. Mathematical model of continuous detonation in an annular combustor with a supersonic flow velocity. *Combust. Explo. Shock Waves* 44(6):690–697.
6. Zhdan, S. A., and A. I. Rybnikov. 2014. Continuous detonation in a supersonic flow of a hydrogen–oxygen mixture. *Combust. Explo. Shock Waves* 50(5):556–567.
7. Fujiwara, T., M. Hishida, J. Kindracki, and P. Wolanski. 2009. Stabilization of detonation for any incoming Mach numbers. *Combust. Explo. Shock Waves* 45:603–605.
8. Liu, S., W. Liu, L. Jiang, and Z. Lin. 2015. Numerical investigation on the airbreathing continuous rotating detonation engine. *25th ICDERS Proceedings*. Leads, England. Paper #157.
9. Wang, C., W. Liu, S. Liu, L. Jiang, and Z. Lin. 2015. Propagation characteristics of continuous rotating detonation wave under different temperature air. *25th ICDERS Proceedings*. Leads, England. Paper #154.
10. Dubrovskii, A. V., V. S. Ivanov, and S. M. Frolov. 2015. Three-dimensional numerical simulation of the operation process in a continuous detonation combustor with separate feeding of hydrogen and air. *Russ. J. Phys. Chem. B* 9(1):104–119.
11. Frolov, S. M., V. S. Aksenov, A. V. Dubrovskii, V. S. Ivanov, and I. O. Shamshin. 2015. Energy efficiency of a continuous-detonation combustion chamber. *Combust. Explo. Shock Waves* 51(2):232–245.
12. Dubrovskii, A. V., V. S. Ivanov, A. E. Zangiev, and S. M. Frolov. 2016. Three-dimensional numerical simulation of the characteristics of a ramjet power plant with a continuous-detonation combustor in supersonic flight. *Russ. J. Phys. Chem.* 10(3):469–482.
13. Frolov, S. M., A. V. Dubrovskii, and V. S. Ivanov. 2012. Three-dimensional numerical simulation of the operation of the rotating detonation chamber. *Russ. J. Phys. Chem. B* 6(2):276–288.
14. Pope, S. B. 1985. PDF methods for turbulent reactive flows. *Prog. Energ. Combust. Sci.* 11:119–192.
15. Bykovskii, F. A., S. A. Zhdan, and E. F. Vedernikov. 2006. Continuous spin detonation of fuel–air mixtures. *Combust. Explo. Shock Waves* 42(4):463–471.
16. Frolov, S. M., V. S. Aksenov, V. S. Ivanov, and I. O. Shamshin. 2015. Large-scale hydrogen–air continuous detonation combustor. *Int. J. Hydrogen Energ.* 40:1616–1623.
17. Frolov, S. M., A. V. Dubrovskii, and V. S. Ivanov. 2013. Three-dimensional numerical simulation of the operation of a rotating-detonation chamber with separate supply of fuel and oxidizer. *Russ. J. Phys. Chem. B* 7(1):35–43.